Control of Gel Morphology and Properties of a Class of Metallo-Supramolecular Polymers by Good/Poor Solvent Environments

Wengui Weng, Zheng Li, Alex M. Jamieson,* and Stuart J. Rowan*

Department of Macromolecular Science & Engineering, Case Western Reserve University, Cleveland, Ohio 44106

Received May 8, 2008; Revised Manuscript Received November 11, 2008

ABSTRACT: Through the utilization of a mixed solvent system, consisting of a good solvent (DMSO) with either a nonsolvent (water) or a poor solvent (ethylene glycol), the morphology and properties of a class of stimuli-responsive metallo-supramolecular gels can be systematically tailored. These gels are formed via self-assembly of a ditopic ligand, consisting of a 2,6-bis(1′-methylbenzimidazolyl)-4-oxypyridine moiety attached to either end of a penta(ethylene glycol) core, in the presence of a transition metal ion (Zn^{II}). In each solvent system, a composition window is located in which gels, varying in turbidity from highly opaque (water- or ethylene glycol-rich) to highly transparent (DMSO-rich), are formed. Morphological observations suggest gelation occurs by a common mechanism throughout the composition range, i.e., via the flocculation of semicrystalline colloidal particles. Increase of DMSO content leads to a reduction in the particle size, accompanied by an increase in sol concentration. WAXD and SAXS analysis indicates that the degree of crystallinity of the colloidal particles is dramatically decreased compared with those formed in a previous study using acetonitrile as solvent but that a new lamellar organization develops as the DMSO content increases, evidently reflecting incorporation of the good solvent into the network structure. These structural changes are accompanied by an increase in the shear storage modulus of the gel up to a maximum value, beyond which the modulus decreases. Thus, by tailoring the solvent composition, it is possible to produce highly transparent gels that, while very strong, are highly mechano-responsive; i.e., they exhibit pronounced yielding and thixotropic behavior.

Introduction

In recent years there has been an enormous growth of interest in the field of supramolecular polymers,[1] which typically consist of chains of small molecules held together by weak reversible noncovalent interactions. The properties of such self-assembled polymers depend on factors such as degree of polymerization (DP), architecture (e.g., linear or branched), and the lifetime of the aggregate, which can be controlled by the binding strength, stoichiometry, and binding kinetics of the supramolecular motif.[2] The dynamic nature of supramolecular polymeric materials allows their behavior to be influenced by external conditions, such as monomer concentration, temperature, and the presence of external fields, in a way that is not possible for traditional covalent macromolecules. Supramolecular polymers thus combine many of the attractive properties of conventional polymers with distinctly new properties that result from the reversibility of the noncovalent bonds between monomeric units and have potential for use as stimuli-responsive materials in fields as diverse as bulk engineering, microscale medicine, and nanotechnology.[3]

A wide range of noncovalent interactions, from simple hydrophobic interactions[4] and $\pi-\pi$ stacking interactions[5] to more complex hydrogen-bonding[6] and metal−ligand interactions,[7,8] can be utilized to build supramolecular polymers. We have focused our attention on metal−ligand interactions that are not only thermodynamically stable but also kinetically labile. The advantages of such metal−ligand interactions, in part, lies in the large catalog of accessible ligands, along with applicable metal ions comprising nearly half the periodic table, which means there are a vast range of metal−ligand complexes that can be easily accessed. The characteristics of a particular metal−ligand supramolecular motif can change dramatically depending on the combination of metal ion and ligand utilized. Significant variations in motif structure (geometry, metal−ligand stoichiometry), dynamics (kinetic lability), and thermodynamic stability can all easily be achieved. Moreover, metallo-organic hybrid polymers offer the attractive possibility of imparting the functional properties of the metal ion,[8,9] e.g., catalysis, light emission, ionic conduction, and gas binding, to the resulting material.

Recently, we have demonstrated that 2,6-bis(1′-methylbenzimidazolyl)-4-oxypyridine (O-Mebip) ligands attached to the ends of a penta(ethylene glycol) core (**1**) result in the formation of metallo-supramolecular gels in acetonitrile upon the addition of transition metal and lanthanide metal ions.[10] These gels were shown to exhibit multiple stimuli-responsive behaviors, including photo-, thermo-, chemo-, and mechanical responses. Under appropriate conditions, transition metal ions such as Zn^{II} or Co^{II} can bind two O-Mebip ligands and thus act as a chain extender to generate linear (or macrocyclic) polymers (or oligomers) of **1** (see Figure 1). Lanthanide ions (e.g., La^{III}, Eu^{III}) can bind one or three O-MeBIP ligands, depending on the binding nature of the counteranions, and thus potentially act as a chain stopper or a trifunctional cross-linker. Therefore, gel properties can be tailored by manipulation of metal ion combinations and taking into account the role of counterion coordination.

Prior studies demonstrated that, in acetonitrile, the gel properties are the result of a phase separation and crystallization process, which produces a dispersion of spherulite-like globular colloidal particles.[10d,e] The interactions between these particles, which may reflect electrostatic forces and metal ion−ligand binding, in addition to the usual van der Waals interactions, give rise to the formation of a network structure. The disruption of this network by mechanical shear, and its facile reformation when shear is removed, are the origin of the pronounced thixotropic behavior of the gels. Here, we are interested in the fact that the **1:Zn** supramolecular polymers are polyelectrolytes in nature and therefore dissolve well in highly polar, coordinat-

* To whom correspondence should be addressed.

10.1021/ma801046w CCC: $40.75
Published on Web 12/04/2008

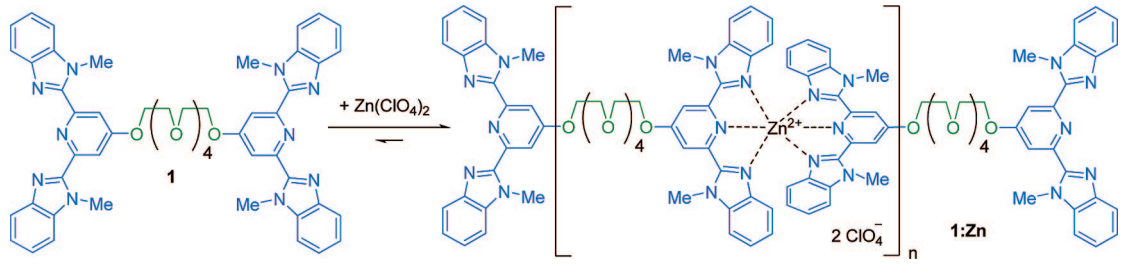

Figure 1. Schematic representation of the formation of metallo-supramolecular polymeric aggregates (**1:Zn**) using ditopic ligand end-capped monomers **1** with metal salts, $Zn(ClO_4)_2$, in various solvents (mixtures).

ing solvents.[11] By adding a cosolvent of different solvation ability, the quality of the solvent can be readily adjusted, offering the ability to tune the phase separation and crystallization process and consequently allow tailoring of the gel formation behavior and stimuli-responsive properties. Mirkin et al.[12] and others[13] have previously reported the preparation of colloidal particles of different metal-containing polymers using controlled precipitation methods. Crystallization and particle fusion and/or flocculation were observed to accompany the precipitation process in some cases. However, in none of these reports was either gel formation or thixotropic behavior reported. Described, herein, is the rational control of the gel morphology, and consequently the properties of these metallo-supramolecular polymers, by simply adjusting solvent quality.

Results and Discussion

Gel Formation in Solvent Mixtures. As mentioned above, all our previous studies on these metallo-supramolecular gels were carried out in acetonitrile.[10] The ligand monomer **1** dissolves fairly well in acetonitrile, with a solubility of ~1 mM. Furthermore, as a consequence of the coordination and solvation effects of acetonitrile, the metallo-supramolecular aggregates **1:Zn**, which form on addition of $Zn(ClO_4)_2$, exhibit enhanced solubility (around 10 mM based on the molar mass of **1**). Increase in **1:Zn** concentration in acetonitrile leads, on cooling from the hot sol, to the formation of precipitate-like materials and eventually strong, opaque gels. Optical microscopy indicates that these gels are composed of relatively large globular particles (ca. 1−50 μm, depending on thermal and mechanical history). As this gel system is based on crystallization of the supramolecular material, it seems reasonable to assume that changing the solvent should lead to dramatic changes in the properties of the gel. Not surprisingly, both the ligand monomer **1** and its metal complexes **1:Zn** are much more soluble in the more polar solvents, dimethyl sulfoxide (DMSO) and dimethylformamide (DMF), and as a consequence no gels could be formed in these solvents. We reasoned that the introduction of a cosolvent, miscible with DMSO or DMF but possessing poorer solvation ability for **1:Zn**, would adjust the solvent quality, which in turn would induce the phase separation/crystallization behavior of the metallo-supramolecular polymer and result in gelation. Furthermore, the different solvents systems may also influence the gel morphology along with the gel's optical and mechanical properties.

In these studies DMSO was chosen as the good solvent for **1:Zn** with the cosolvents being either water (a nonsolvent for **1:Zn**) or ethylene glycol (a poor solvent for **1:Zn**). A series of **1:Zn** gels were prepared using different combinations of DMSO/water and DMSO/ethylene glycol mixtures. Figure 2 shows the gels (concentration of 50 mg/mL) formed at three different solvent compositions for the two mixed-solvent systems. As can be seen in both cases, increasing the ratio of DMSO to the cosolvent leads to decrease in opacity. In addition, an increase in gelation time, the time required for a gel to form

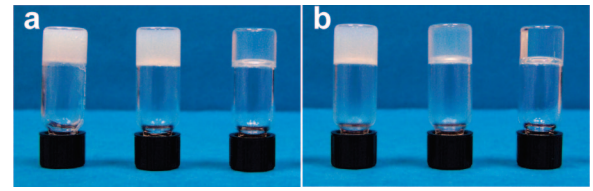

Figure 2. Gelation of **1:Zn** metallo-supramolecular polymers in mixed solvents: (a) from left to right, DMSO/water in ratios of 60/40, 70/30, and 80/20 (v/v); (b) from left to right, DMSO/ethylene glycol in ratios of 40/60, 50/50, and 60/40 (v/v). Gel concentration is 50 mg/mL.

from a clear hot sol while being cooled to room temperature under ambient conditions, as the DMSO fraction is increased is also observed. Specifically, for the DMSO/water system, the gelation time increases from a few minutes to around a half-hour as the DMSO/water ratio is increased from 60/40 to 80/20 (v/v). Similarly for the DMSO/ethylene glycol systems the gelation time increases from a few minutes to around one and half hours as the DMSO/ethylene glycol ratio is increased from 40/60 to 60/40 (v/v). It should be noted that the gelation time is dependent on the thermomechanical history, and the higher the DMSO content, the stronger this dependence appears to be. Quenching (by placing the sample vial in an ice bath) and/or shaking the sample leads to faster gelation. Such effects were observed in our previous studies of gelation of **1:Zn** in acetonitrile[10] and may be accounted for by a thermomechanical history-dependent nucleation process.[14]

At a specific **1:Zn** concentration, gelation occurs only over an intermediate range of solvent combinations. For example, for the DMSO/water system, at a concentration of 50 mg/mL, if the DMSO fraction is lower than 50% only precipitate is obtained, while if the DMSO fraction is larger than 82.5% only clear sols are formed. Similar results are observed for the DMSO/ethylene glycol system, at 50 mg/mL, with the lower and upper bounds for gelation occurring at DMSO fractions of 30% and 65%, respectively. In addition, gelation is concentration dependent; i.e., it is possible only at sufficiently high concentrations for a specific solvent composition (see Supporting Information). For example, when a 50/50 (v/v) DMSO/ethylene glycol mixture is used, gels with a concentration as low as 20 mg/mL can be obtained with the gelation time and gel transparency increasing as concentration is decreased. On the other hand, the lowest concentration at which a gel is obtained, when a 60/40 (v/v) DMSO/ethylene glycol mixture is used, is around 40 mg/mL. The solubility of **1:Zn** in DMSO could not be determined because of sample limitations but is in excess of 200 mg/mL. On the basis of these experimental observations, it is possible to construct portions of a schematic phase diagram for the **1:Zn**/DMSO/ethylene glycol system (Figure 3) in which the solid lines delineate known sol−gel boundaries, and broken lines denote hypothetical boundaries, drawn by extrapolation from the experimental results. Thus, by adjusting solvent quality, using a combination of a good solvent with a nonsolvent or a poor solvent, the gelation process can be readily manipulated

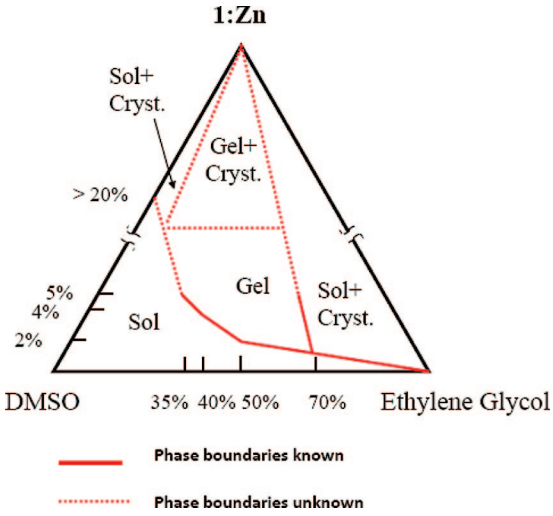

Figure 3. Ternary phase diagram for the **1:Zn**/DMSO/ethylene glycol system: the lower portion indicates solid lines, which connect points based on experiments described in the text; the upper portion is speculative. As a consequence of sample limitations, it was not possible to locate the solubility limit of **1:Zn** in DMSO, which is greater than 20% w/v.

to control a range of gel properties, such as the gelation time, gel transparency, and, as we will show, gel morphology and thermomechanical response.

Optical Microscopy of Gels. Microscopic analysis of gel morphology can yield insight into the gelation mechanism and origin of the gel properties.[15] Previous microscopy studies have shown that the gels formed by **1:Zn** in acetonitrile consist of semicrystalline globular colloidal particles.[10d,e] As mentioned above, the use of the mixed solvents to adjust the solvent quality resulted in a dramatic change in the optical properties and formation kinetics of these gels. To investigate the reason for this change, as well as to see whether the gelation mechanism is similar to that previously observed in acetonitrile, a series of microscopic studies using differential interference contrast (DIC) and polarized (POM) optical microscopy techniques were carried out on the gels.

Figure 4 shows the DIC and POM images of three gels in DMSO/water mixtures of compositions 60/40, 70/30, and 80/20 v/v. These images span the concentration window which defines the gelation regime in the 1:Zn;DMSO:water system, which, as noted above, ranges from 50 to 82.5 vol % DMSO. Globular particles are clearly apparent, particularly in the opaque gels (compositions 60/40 and 70/30 v/v). The particle sizes decrease from an average diameter of around 70 μm to smaller than 5 μm, as the DMSO/water ratio is varied from 60/40 to 80/20 (v/v). As seen by comparing with Figure 2a, this trend coincides with a decrease in the opacity of the gel samples; i.e., less opaque gels with higher DMSO fractions have smaller particle sizes (vide infra). Polarized optical microscopy reveals distinct Maltese cross figures associated with the globular particles, indicative of a spherulite texture. These are particularly evident in Figure 4b and to a lesser extent in Figure 4d but are not seen in the most transparent sample (Figure 4e), although some birefringent areas are apparent. The trend suggests a loss of order as the solvent quality improves. Similar features were observed in the microscopic images of gels in DMSO/ethylene glycol mixtures (see Supporting Information). These microscopic studies indicate that the gelation mechanism in the more turbid gels is similar to that in the acetonitrile gels;[10d,e] i.e., gelation occurs on cooling from the hot sol, through formation of colloidal particles via crystallization of the supramolecular polymer.

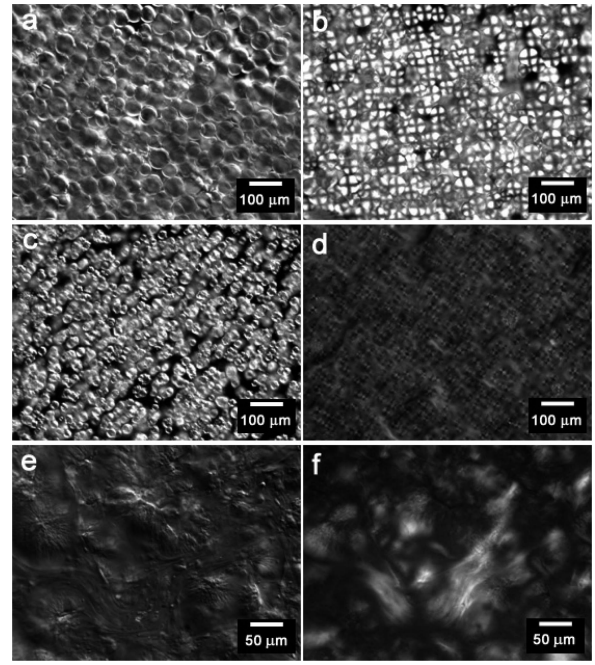

Figure 4. Optical microscopy of three gel samples of **1:Zn** formed in various DMSO/water mixtures as shown in Figure 2a. Differential interference contrast (DIC) images of (a) 60/40, (c) 70/30, and (e) 80/20 (v/v) and their corresponding polarized images (b), (d), and (f).

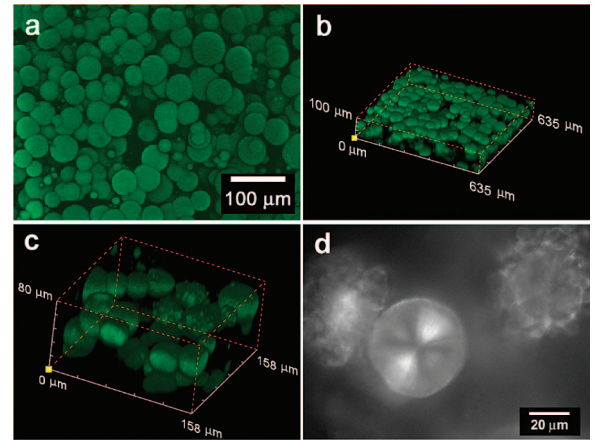

Figure 5. Laser scanning confocal microscopy (LSCM) images (a) *z*-projection image, (b) 3D image of the **1:Zn** gel formed in 60/40 (v/v) DMSO/water mixture as shown in Figure 2a, and (c) LSCM and (d) polarized images of the **1:Zn** gel formed in 70/30 DMSO/water mixture (v/v) showing the coexistence of regular and irregular particles.

The three-dimensional structure of the gels in these mixed solvents can be observed by taking advantage of the fluorescent properties of **1:Zn** and using laser scanning confocal microscopy (LSCM). Thus, for the gel formed in 60/40 (v/v) DMSO/water, from either the *z*-projection image (Figure 5a) or the 3D image (Figure 5b), an interconnected colloidal microstructure is exhibited, consisting of globular particles in contact with each other and permeated by solvent channels. In some cases, it appears that the globular particles are deformable and able to interpenetrate at the area of contact. This further exemplifies that gel formation is the result of flocculation of the globular particles. It should be noted that the extraction of a sample of the gel for microscopic examination involves mechanical perturbation of the sample, and so the observed structure may not fully reflect the nascent network organization of the gels.

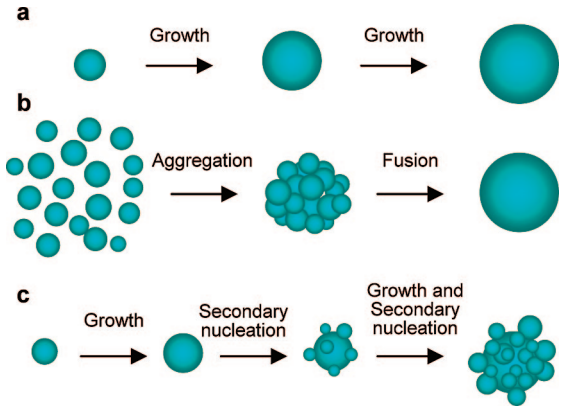

Figure 6. Possible mechanisms for formation of particles of metallo-supramolecular polymers from solution. (a) Large uniform particles via growth from a single nucleus. (b) Small particles form initially, subsequently aggregate into clusters, which then slowly anneal into single uniform spherical particles through intraparticle fusion. (c) Nucleation and growth of primary particles, followed by secondary nucleation of particles on the growth surface of primary particles, resulting in large irregular particles.

Previously, we observed that, in the acetonitrile gels, the particles are often very irregular in shape, sometimes with sharp edges, and appear to be composed of very small primary particles.[10e] Close examination indicates that, in the mixed solvent systems, some particles are also irregular in shape. As an example, higher magnification images from the 70/30 DMSO/water (50 mg/mL) gel are shown in Figure 5c,d. In these gels uniform and irregular particles coexist, and the latter clearly seem to be composed of multiple smaller particles (Figure 5c). In addition, the regular particles appear to be more crystalline, as indicated by the stronger birefringence in the POM images (Figure 5d). In general, simultaneous formation of uniform and irregular particles can be visualized to occur in several ways as depicted in Figure 6. Large uniform particles could clearly form via radial crystal growth from a single nucleus (Figure 6a). Alternatively, such particles could form through agglomeration of primary particles, which subsequently anneal into a single uniform spherical particle via intraparticle fusion, as proposed by Mirkin and co-workers[12a] (Figure 6b). If the fusion process is quenched in an intermediate state or if it occurs very slowly, then irregular particles would be observed. Finally, secondary nucleation and growth of small particles directly on the surface of a primary particle is also possible (Figure 6c).

In an attempt to gain more insight into the particle formation process, time-resolved optical microscopy was carried out on a gel formed in 70/30 DMSO/water (50 mg/mL). In a typical experiment, a gel sample was loaded into a planar glass cell and heated to dissolution. On removal of the heat source, the specimen was immediately imaged at an acquisition rate of 24 frames/s for a prolonged period of time. For simplicity, the starting point was set at the time when the first image was acquired, although it takes ca. 10 s to mount the sample on the stage and to adjust the stage position after removal from the heat source. After a very short induction period of ~8 s (see Supporting Information), a few globular particles were observed to nucleate and increase rapidly in size during the subsequent 10 s. Within 1 min, a metastable morphology of dense particles is attained, corresponding to a space-filling gel network, with cluster sizes (of around 30 μm) comparable to that of the large particles (both regular and irregular) grown in a sample vial. After 1 min, very little noticeable change in the morphology can be discerned. The time elapsed during the induction period and formation of a mature gel network is much shorter than when the same gel is formed in a sample vial, which usually takes ca. 10 min. Particles which have uniform spherical shapes

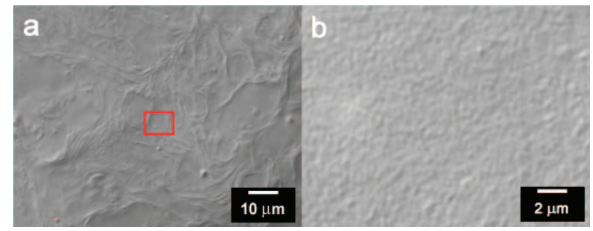

Figure 7. Laser scanning transmission microscopy images of a **1:Zn** gel (50 mg/mL) formed in 60/40 (v/v) DMSO/ethylene glycol mixture as shown in Figure 2b. (b) is the zoom-in of the rectangular region highlighted in (a).

predominate only at the earliest stages of phase separation and subsequently are observed as rare, isolated particles in the later stages of phase separation. This contrasts with gels grown in a sample vial, in which such particles are more frequently observed in mature gels. The uniform particles at early stages of gelation have sizes of the order of 5 μm, comparable to the small particles which agglomerate into the very large irregular particles seen in gels grown in a sample vial (Figure 4) and thus could be regarded as primary particles. The short induction time, rapid particle growth, and predominance of irregular particles are likely the result of the more efficient heat transfer in the thin cell used in the optical microscopy experiments (depth of ca. 200 μm and small sample volume (ca. 20 μL)). This results in a very rapid quench, and very fast nucleation and growth of particles, on removal from the heat source.

It is unclear from the time-resolved microscopy observations (see Supporting Information) whether the process of particle fusion, envisaged by Mirkin et al.,[12a] occurs in these gels. Certainly, no such events were identified in these time-resolved experiments. However, such a two-step fusion mechanism could occur between nanoscale particles in the very early stages of the gelation process and would not be observed because of the limited resolution of the optical microscopy technique. Nevertheless, it seems clear that two of the processes visualized in Figure 6a,c are present at the micron scale, i.e., (i) nucleation and growth of large spherical particles and (ii) nucleation and growth of primary particles, followed by secondary nucleation of particles on the growth surface of primary particles. The first process will be more prevalent under conditions where the nucleation rate is relatively slow and will lead to large uniform spherical particles, while the second process will be more prevalent under conditions where rapid nucleation and growth occurs and will result in large irregular particles. Parenthetically, another path to irregular particles, observed in the time-resolved microscopy throughout the gelation process, involves the impingement of growing near-neighbor particles.

It seems likely that the gelation mechanism in the more transparent gels is also colloidal in nature, but this cannot be confirmed based on optical microscopy. For example, as shown in Figure 7, the laser scanning transmission images at highest resolution of the highly transparent gels (50 mg/mL) formed in 82.5/17.5 DMSO/water mixture and 60/40 DMSO/ethylene glycol indicate small particle sizes of around 500 nm. No colloidal structure can be revealed by optical microscopy for even more transparent samples, e.g., 40 mg/mL in 60/40 DMSO/ethylene glycol, 50 mg/mL in 65/35 DMSO/ethylene glycol, and 50 mg/mL in 82.5/17.5 DMSO/water. In an attempt to address this issue, a series of dynamic light scattering (DLS) experiments were carried out. For example, DLS studies on a sol, prepared from a 50 mg/mL **1:Zn** gel in 60/40 DMSO/ethylene glycol which was diluted to 20 mg/mL and sonicated,[10d] contained 523 ± 82 nm particles (comparable to the size estimated from optical microscopy), while a similar experiment on a sol (same solvent) formed from a gel containing

Table 1. 1:Zn Gel Melting Temperature Obtained from Differential Scanning Calorimetry Study[a]

	DMSO/water			DMSO/ethylene glycol		
ratio (v/v)	60/40	70/30	80/20	40/60	50/50	60/40
T_m (°C)	82.6 ± 6.2	70.1 ± 0.4	50.9 ± 0.7	72.9 ± 2.1	57.0 ± 0.6	47.3 ± 1.7

[a] The results are the average of at least three runs.

40 mg/mL **1:Zn** yielded a particle size of 143 ± 32 nm upon dilution to 33 mg/mL, suggesting that preparation of gels with particle sizes comparable to or smaller than 100 nm seems highly possible.

An important point to be noted here is that the particle sizes in the turbid gels can be decreased dramatically, to values comparable to those obtained in the DMSO-rich mixed solvents, by sonicating the sample during cooling of the hot sol.[10d,e] While this substantially enhances the mechanical strength of the gels, it does not decrease significantly the turbidity. This strongly suggests that the increased optical clarity of the gels with a larger DMSO content is on account of a reduction in the refractive index contrast between the gel particles and the mixed solvent systems, presumably originating in the incorporation of the good solvent DMSO into the gel particles.

Differential Scanning Calorimetry and Wide-Angle X-ray Diffraction Analysis. A key question in these studies was how the use of mixed solvents influences the crystallinity of the **1:Zn** gels and to see whether any effects could be correlated with the morphological changes observed in the microscopy studies above. First, the melting temperatures, T_m, of the gels were determined as a function of the solvent composition, using differential scanning calorimetry (DSC) performed in hermetically sealed DSC pans. The maxima of the DSC melting peaks are identified as the gel melting temperatures, T_m, and the resulting values are listed in Table 1. Clearly, Table 1 indicates that, for both mixed-solvent systems, increase in DMSO content leads to a decrease in T_m. A more careful examination of the DSC data (Supporting Information) shows that, for the opaque gels (in 60/40 DMSO/water and 40/60 DMSO/ethylene glycol), the melting peaks are small but quite sharp. However, upon increasing the DMSO content, the peaks become much broader and appear to occur at lower temperatures. In general, these features reflect the low concentration (50 mg/mL) and/or low crystallinity of the gels and further suggest a decrease in crystalline order with increase of DMSO content. Wide-angle X-ray diffraction (WAXD) patterns for gels with different solvent compositions are essentially identical and feature prominently an amorphous halo, centered at a *d*-spacing of 0.45 nm, together with a very weak peak at a *d*-spacing of 0.96 nm (see Supporting Information), seen in earlier studies of **1:Zn** in acetonitrile and suggested to relate to the stacking of O-Mebip:Zn complexes.[10e] Comparison of the WAXD patterns obtained in the mixed solvents versus those obtained in acetonitrile[10d,e] indicates the degree of crystallinity is drastically reduced in the presence of DMSO. Thus, taken together the data suggest that enhanced solvent quality, through addition of DMSO, results in gels with increased transparency (tied to lower refractive index contrast), a decrease in T_m, a broadening of the melting peak, and reduced crystallinity, which are all reflective of increased structural disorder in the gels.

Small-Angle X-ray Scattering (SAXS) Analysis. To gain further insight into the structural changes in the metallo-supramolecular gels, which accompany the addition of a good solvent, SAXS studies were performed on the six gel systems: **1:Zn** in DMSO/water at ratios of 60/40, 70/30, and 82.5/17.5 v/v and **1:Zn** in DMSO/ethylene glycol at ratios of 40/60, 50/50, and 60/40 v/v, in each case the gel concentration being 50 mg/mL. For each solvent system, the three compositions reflect changes in optical quality from opaque, to translucent, to transparent (cf. Figure 2) and morphological changes in optical microscopy from large spherulites to smaller spherulites to featureless. In Figure 8, we show the SAXS results, which indicate evolution of a lamellar structure as the DMSO content of the solvent increases. This is indicated by the appearance in both solvent systems of two peaks located near $q = 0.8$ and 1.6 nm^{-1}, i.e., a peak spacing of 1:2, corresponding to a lamellar *d*-spacing of ~8.0 nm.[16]

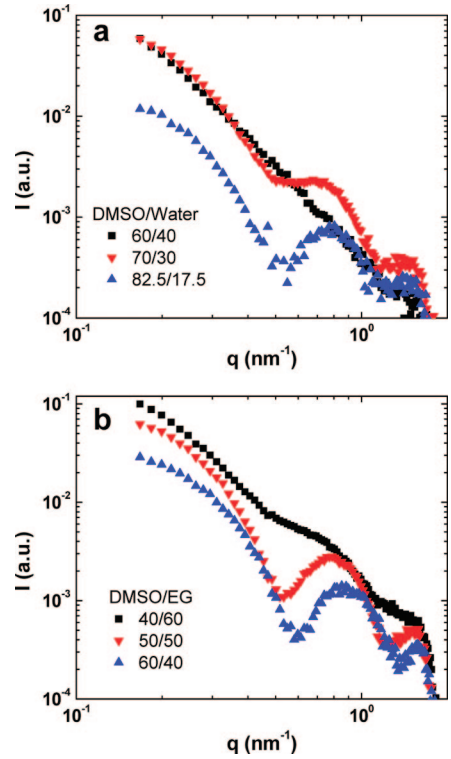

Figure 8. Small-angle X-ray scattering (SAXS) of samples formed in (a) DMSO/water and (b) DMSO/ethylene glycol mixtures, at different solvent compositions. The ratio of DMSO to cosolvent (v/v) is indicated in the figure; the gel concentration is 50 mg/mL.

The nature of this lamellar structure is not clear, but noting that the periodicity is ~3 times the length of a fully stretched ditopic monomer, it appears to involve nanosegregation of the metallo-supramolecular polymer. Several possibilities can be envisaged. One recognizes that the chain ends of the polymer are relatively hydrophobic, and so segregation may occur into metallo-supramolecular polymer layers, in which water or ethylene glycol may be segregated into the pentaethylene oxide cores, separated by layers of the more organophilic solvent, DMSO. Another possibility may be chain-folded metallo-supramolecular polymer layers, in which the lamellar surfaces are pentaethylene oxide folds, again separated by solvent layers. A third possibility relates to the fact that increasing the DMSO content of the solvent leads eventually to the formation of a sol phase. Thus, it seems possible that the lamellar organization might consist of phase-separated metallo-supramolecular gel layers, separated by layers of a dilute sol phase.

Linear Viscoelasticity of the Gel Network. Studies were next carried out to elucidate how the mechanical properties of the **1:Zn** gels are affected by the solvent content, beginning with the linear viscoelastic behavior. Efforts were made to

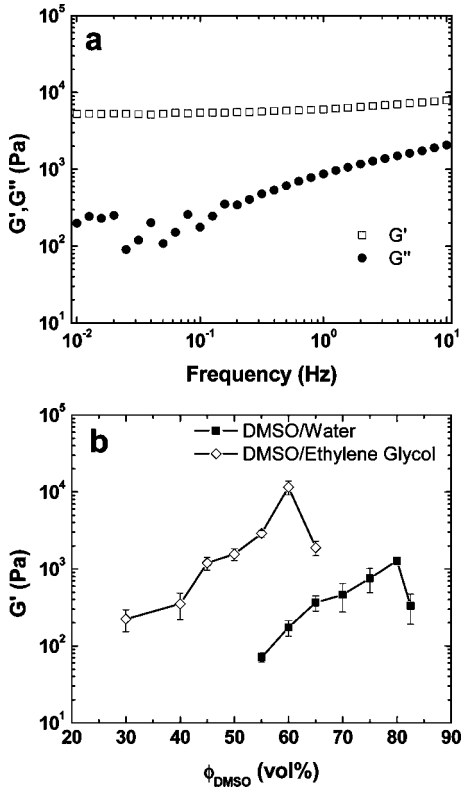

Figure 9. (a) Frequency-dependent storage and loss moduli of a clear **1:Zn** gel formed in 60/40 (v/v) DMSO/ethylene glycol mixture (concentration: 50 mg/mL). (b) The storage modulus values, taken at a frequency of 1 Hz, of various **1:Zn** gels from the frequency sweep measurements. The shear strain applied is 0.2%, and the gel concentration is 50 mg/mL.

correlate the mechano-responsive behavior with the variation in particle size and particle volume fraction of the gels.[17] Specifically, the goal here was to examine how gel strength can be tailored by varying solvent quality. Measurements of storage and loss moduli, $G'(\omega)$ and $G''(\omega)$, respectively, were carried out as a function of the oscillatory deformation frequency, ω. A transparent gel sample in 60/40 DMSO/ethylene glycol was loaded in the rheometer as a clear sol and subjected to oscillatory shear (strain $\gamma = 0.2\%$, deformation frequency $\omega = 1$ Hz) for 4 h to allow for completion of gelation; then G' and G'' were determined as a function of frequency at a fixed strain amplitude of 0.2%, well within the linear viscoelastic regime. As shown in Figure 9a, the measured values of G' (open symbols) are essentially constant at low frequency and are approximately an order of magnitude larger than G'' (solid symbols) over the entire frequency range, confirming that this transparent gel has a highly elastic network.[18] Similar overall behavior was observed for the other solvent compositions. Figure 9b shows the storage modulus values, taken at room temperature and a frequency of 1 Hz, of the various **1:Zn** gels in DMSO/water and DMSO/ethylene glycol, as a function of solvent composition. In both systems, the gel modulus increases with DMSO content to a point where a maximum value is obtained. At that point a slight increase in DMSO ratio results in a decrease in the gel modulus, and finally, at even higher ratios of DMSO, a transparent sol is obtained. It is observed that for each mixed-solvent system the maximum in modulus occurs where the gels are highly transparent. These observations are consistent with the colloidal nature of the gels and the fact that the particle size decreases with increasing transparency, although, based on the SAXS and DLS evidence, a transformation from spherical (onion-like) to an exfoliated lamellar organization cannot be excluded.[16] Colloidal gels composed of smaller

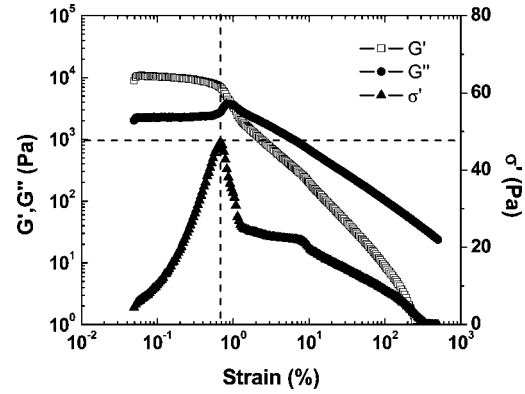

Figure 10. Strain sweeps showing the crossover from linear to nonlinear viscoelasticity of the transparent **1:Zn** gel formed in a 60/40 (v/v) DMSO/ethylene glycol mixture (concentration: 50 mg/mL). The shear frequency applied is 1 Hz.

particles typically have a higher modulus because they have a larger specific surface area, and hence more interparticle interactions are expected, leading to higher gel strength.[19] The decrease in gel strength upon further addition of DMSO is presumed to reflect a decrease in particle volume fraction as a consequence of a higher sol content. At the gel concentration (50 mg/mL) under investigation, the range of DMSO content at which a gel can form at room temperature is 50−82.5 vol % for the DMSO/water system and 30−65 vol % in the case of DMSO/ethylene glycol. This is consistent with the difference in solvent quality between water, a nonsolvent, and ethylene glycol, a poor solvent, for **1:Zn**.

From the above studies, it is clear that, by manipulating the solvent quality, it is possible to tailor the microscopic structures as well as the optical, thermal, and mechanical properties of these metallo-supramolecular gels. Specifically, it is possible to prepare highly transparent gel samples which are mechanically strong. Such properties could be important for potential applications as stimuli-responsive optical coatings.

Nonlinear Viscoelasticity of the Gel Network. Also important to potential coatings applications of these gel systems are the nonlinear viscoelasticity and thixotropy associated with respectively the breakup and reformation of the gel network under large mechanical deformations. Figure 10 shows double-log plots of the storage and loss moduli for the transparent gel formed in 60/40 (v/v) DMSO/ethylene glycol mixture as a function of the strain amplitude at a deformation frequency of 1 Hz. The results show a distinct linear viscoelastic region is present at low strains, where log G' and log G'' remain essentially constant up to a critical strain of around 0.5%, beyond which log G' decreases abruptly, while log G'' increases slightly to a maximum value and then decreases albeit less rapidly than log G'. Thus, a crossover of G'' is observed at a strain of ~0.91%, after which G'' becomes increasingly larger than G', indicative of the onset of viscous flow at large strains. The high equilibrium modulus, narrow linear viscoelastic regime, and small strain at which onset of viscous flow occurs exemplify that this transparent gel is very strong, but brittle. Similar behavior has been documented in a variety of colloidal gel systems.[20−23]

In a thixotropic material, when subjected to shear deformation, one expects a competition between bond breaking, which occurs as a consequence of the action of shear forces, and bond formation, which occurs on account of convective collisions between separated elements.[24,25] The initial increase of G'' with strain in the low strain range, evident in Figure 10, is thus attributed to breakdown of agglomerates into smaller-sized units, resulting in a more dissipative system. At higher strains, further

breakdown of the structure leads to shear-thinning viscous flow behavior. Indeed, the maximum in loss modulus and the thixotropic behavior is consistent with a model proposed by Yziquel et al.,[21] in which the competition between breakdown and buildup of the microstructure is attributed to hydrodynamic forces and Brownian motion, respectively, which results in the characteristic nonlinear behavior under shear deformation as seen in Figure 10.

It is of interest to determine the yield stress of the gel, which provides a measure of the force needed to break down the gel microstructure. For a colloidal gel formed by flocculated particles, the yield stress has been related to the maximum force per unit area that the network can withstand before rupturing.[26] A number of different methods are available to ascertain the yield stress of a gel. One approach utilizes a yield criterion introduced by Bingham[27] which allows one to acquire an estimate of the yield stress from steady shear experiments.[10d] Alternatively, the yield stress can be estimated from creep experiments, as detailed below. Also, from the oscillatory strain sweep experiments (Figure 10), one expects that the shear stress stored by the network will increase with strain magnitude up to the yield point, after which it will decrease because some portion is expended in disrupting the network. Thus, a distinct maximum should be observed in the elastic stress, as the strain is increased, the value of which may be equated to the yield stress.[22d,28] Indeed, such behavior is observed for the metallo-supramolecular gels by plotting the elastic stress, $\sigma' = G'\gamma$, vs shear strain (Figure 10). Thus, it can be deduced (see the dashed lines in Figure 10) that the yield point occurs at a yield stress (σ_y) of 47 Pa and a yield strain (γ_y) of 0.69%, the latter being slightly smaller than the strain where the crossover in G' and G'' occurs.

To gain further insight into the origin of the nonlinear viscoelastic response of the transparent gel, creep experiments were also performed, and the corresponding creep and creep recovery data (as a function of the applied stress, σ_0) are shown as time-dependent strain, $\gamma(t)$ (Figure 11a) and shear compliance, $J(t) = \gamma(t)/\sigma_0$ (Figure 11b), respectively, plotted against elapsed time, t. In these experiments, the specified stress was applied for 120 s, and the strain recovery after removal of the stress was monitored for a further 120 s. As an aid to interpreting these data, Figure 12 illustrates schematically the creep and recovery curves for a typical nonlinear viscoelastic material. The time dependence of shear strain (γ) can be expressed as follows:

$$\gamma(t) = \gamma_s + \gamma_d(t) + \gamma_v(t) \quad (1)$$

where γ_s is the instantaneous strain, $\gamma_d(t)$ a retarded elastic strain, and $\gamma_v(t)$ the viscous flow. For nonlinear viscoelastic materials, the instantaneous strain γ_s may, in principle, consist of an elastic component, γ_e, and a plastic component γ_p. γ_e and $\gamma_d(t)$ are fully recoverable upon unloading the stress; $\gamma_v(t)$ and γ_p are not recoverable after unloading.

Comparing Figures 11a and 12, it can be seen that, at small applied stresses, up to 10 Pa, the **1:Zn** clear gel, formed in 60/40 (v/v) DMSO/ethylene glycol, exhibits a highly elastic behavior, as indicated by the fact that $\gamma_s \approx \gamma_e$, $\gamma_v(t)$ and $\gamma_p \approx 0$, and there is a negligible amount of permanent set in the recovery phase, $\gamma_r \approx 0$. The total strain reaches a constant value after 120 s, from which the equilibrium compliance J_e may be determined, $J_e = 0.189$ kPa^{-1}. The corresponding value for the equilibrium shear modulus, $G_e = 1/J_e$, is thus estimated to be 5.30 kPa, a value very consistent with values of the storage modulus (5.25 kPa) in Figure 9a at lowest frequency. Thus, the controlled-strain and controlled-stress experiments are self-consistent. As the stress is increased up to 40 Pa, small amounts of viscous flow develop and permanent set increases. When the

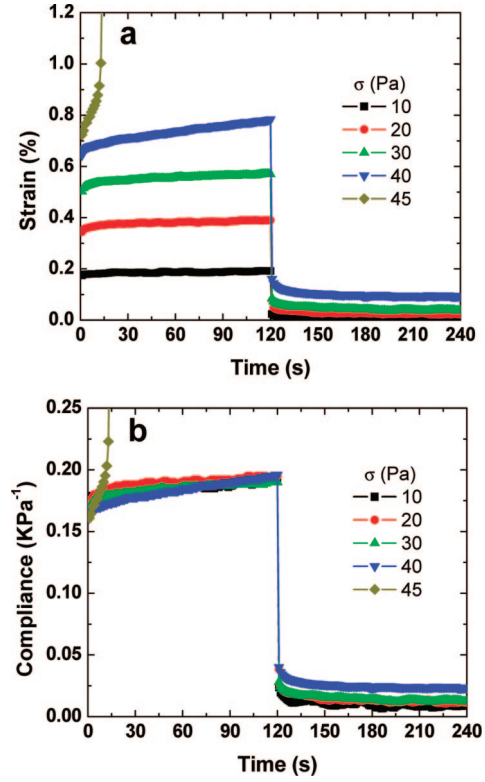

Figure 11. Creep and recovery curves of the **1:Zn** clear gel formed in 60/40 (v/v) DMSO/ethylene glycol mixture (concentration: 50 mg/mL) for various applied stress values as indicated: (a) time-dependent strain deformation, $\gamma(t)$; (b) time-dependent shear compliance, $J(t)$. The stress was applied for 120 s, and the recovery after removal of the stress was monitored for a further 120 s.

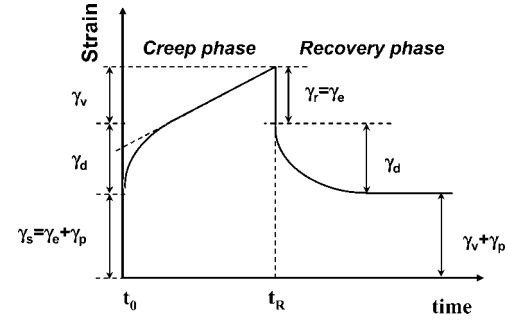

Figure 12. Schematic illustration of the creep and recovery behavior of a nonlinear viscoelastic material.

applied stress is increased from 40 to 45 Pa, a striking change occurs, as seen in Figure 11. At the higher stress, the sample flows as a viscous fluid with deformation and compliance dramatically increasing with time. Note from Figure 11a that the applied stress level of 45 Pa is very close to the yield stress, $\sigma_y = 47$ Pa, and the strain at yield (0.73%) is essentially identical to the yield strain $\gamma_y = 0.69\%$, estimated from the oscillatory strain sweep experiment (Figure 10), again indicating self-consistency between the controlled-strain and controlled-stress experiments. The viscosity associated with the initial flow accompanying yield can be estimated to be around 310 kPa·s corresponding to a constant shear rate of around 1.4×10^{-4} s^{-1}. Also interesting to note in the creep curve for 45 Pa is a distinct flow transition at a strain of around 0.90%, where the rate of deformation increases enormously, and the viscosity drops significantly. This indicates strongly that shear-thinning flow occurs at a strain comparable to that where the $G'-G''$ crossover occurs in the oscillating strain sweep measurements

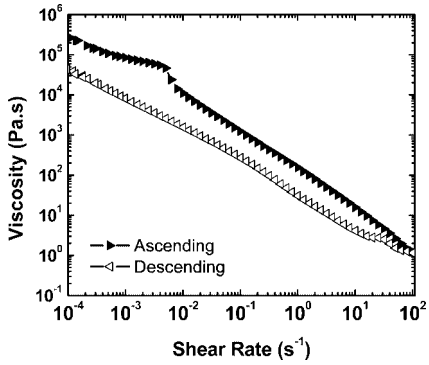

Figure 13. Thixotropic loop experiment plotted as viscosity against shear rate for the transparent **1:Zn** gel formed in 60/40 (v/v) DMSO/ethylene glycol mixture (concentration: 50 mg/mL). The loop test was conducted by ramping shear rate from 10^{-4} to 100 s^{-1} and then back to 10^{-4} s^{-1} in a time period of 120 s.

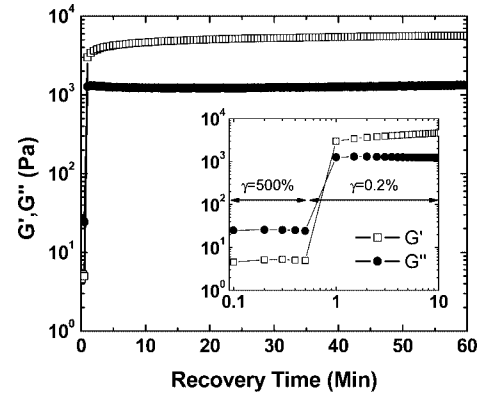

Figure 14. Plot of gel network restoration after preshear, of the clear **1:Zn** gel formed in 60/40 (v/v) DMSO/ethylene glycol mixture (concentration: 50 mg/mL). Inset shows the immediate reformation of gel network and the effective preshear treatment.

(Figure 10). In summary, the picture that emerges from these viscoelastic studies is that the gels are strong but highly responsive, in the sense that they fail at a relatively small yield stress and yield strain. In concluding this section, we note that the clear gels formed in DMSO/water demonstrated similarly elastic behavior in creep tests and, moreover, that the turbid gels, obtained at lower DMSO content in both solvent systems, show essentially identical creep responses, exhibiting large recoverable strains (see Supporting Information). Thus, we observe no change with variation of solvent composition in the essential character of the viscoelastic response of these materials, despite the manifest changes in structural organization and optical clarity. It is pertinent to note here that Daniels et al.[29] have suggested on the basis of a compressive creep test that gel-like systems containing spherulitic particles cannot be considered true thermoreversible gels since they do not show elastic recovery in a compressive creep test. Our shear creep results definitively show that such systems do exhibit elastic recovery when they are subjected to strains below the yield strain and therefore are indeed true gels.

Thixotropic Behavior. As seen above, and akin to the **1:Zn** gels in acetonitrile,[10d,e] the gels formed in mixed solvents show pronounced thixotropic behavior; i.e., application of shear or shaking leads to the formation of a free-flowing liquid, which rapidly reforms into the gel state upon standing. To quantitatively evaluate this behavior, a shear rate loop test was applied to the transparent gel (50 mg/mL in 60/40 (v/v) DMSO/ethylene glycol mixture), and the resulting viscosity−shear rate relationship is shown in Figure 13. The low-shear viscosity is very high, in the range of 250 kPa·s, which is comparable to the steady shear viscosity estimated from the creep experiments in Figure 11 (310 kPa·s). An apparent flow transition is observed on the ascending shear curve, which could be a result of a yield occurrence or, alternatively, to the onset of wall slip between the rheometer plates and the sample,[30] which is a common problem encountered in rheology of concentrated colloidal dispersions.[31−34] It should be noted in Figure 13 that, prior to the transition, the magnitude of the shear stress increases to a level higher than the yield stress and that the stress remains higher at ∼100 Pa on the ascending part of the loop, after the transition. Before this critical transition point only a limited amount of flow occurs, whereas when the shear rate is increased beyond this point, the gel thins catastrophically, as indicated by the power-law decrease in viscosity. Upon reversing the stress, the viscosity increases with decreasing shear rate, but with a significant hysteresis, reflecting a time lag in reformation of the gel network structure. This thixotropic behavior is similar to the acetonitrile gel,[10d] except for the apparent flow transition observed here. The use of a mixed solvent system allows the systematic tailoring of the yield behavior (vide supra), and thus the details of the thixotropic loop can be manipulated by varying solvent composition. Thixotropic behavior can be important for coatings applications, where low viscosity is required to allow ease of application, but a delay in recovery of viscosity allows for film leveling and consolidation.

Gel Recovery Kinetics. Having explored the yield behavior and thixotropy of the transparent gel formed by **1:Zn** in 60/40 DMSO/ethylene glycol, an investigation of the kinetics of gel recovery was undertaken. The recovery process was monitored by a rheological experiment conducted under oscillatory shear. A gel sample, formed in the rheometer by a procedure identical to that used for the frequency sweep experiment, was subjected to a large-strain preshear, 500% strain at a frequency of 1 Hz, for 30 s, following which the recovery was monitored in the linear viscoelastic regime by immediately stepping down to a small oscillatory strain of 0.2%, also at a frequency of 1 Hz. The resulting time evolution of storage modulus (G') and loss modulus (G'') are shown in Figure 14. Consistent with visual observation, reconstitution of a partially developed network occurs within 30 s, as indicated by the crossover of storage modulus and loss modulus ($G' > G''$), and the equilibrium storage modulus value characteristic of the fully developed network is almost reached ($G' \sim 5.6$ kPa) after 45 min. The initial storage modulus at 30 s after cessation of preshear is around 3.0 kPa, corresponding to about 54% of the equilibrium modulus. Also, during the preshear at large strain (inset in Figure 14), both G' and G'' are small, with $G' < G''$, and are essentially constant, confirming that dynamic preshear at large strain amplitude is effective in breaking the gel network. The fast breakdown under shear and rapid reformation of gel state could be of great importance to the processing of the material into complex shapes using colloidal processing techniques such as gel casting,[35] injection molding,[36] direct writing,[37] and so on.

Gel Formation Kinetics. It is also important to know the kinetics of gel formation from the sol state. Again, the transparent gel formed by **1:Zn** in 60/40 DMSO/ethylene glycol was used as an example for this study. The gelation process was monitored by a rheological experiment conducted under oscillatory shear at a strain (0.2%) well within the linear viscoelastic regime of a full developed gel. Typically, a clear gel was dissolved by heating at 120 °C for 150 s to ensure complete dissolution of the colloidal particles and then loaded onto the rheometer after being cooled down to room temperature at ambient conditions for 5 min. The storage and loss moduli were monitored by a time sweep as in the study of gel recovery kinetics. Within 30 s after the time sweep started gel network

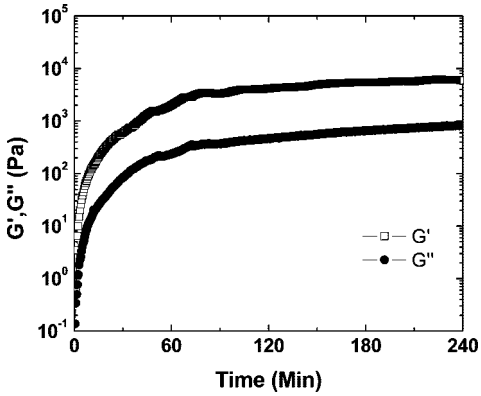

Figure 15. Kinetics of formation of a transparent **1:Zn** gel from a clear sol in a 60/40 (v/v) DMSO/ethylene glycol mixture at a concentration of 40 mg/mL, monitored by following the increase in shear moduli.

formation has occurred, as indicated by the fact that $G' > G''$ (Figure 15), and an equilibrium state is reached in ~90 min.

Since crystallization accompanies gelation, it follows that there are at least four processes involved in gel formation, i.e. nucleation, particle growth, flocculation, and coalescence to form a three-dimensional network. The gel recovery study discussed above suggests that once particles are formed, flocculation is very fast. Thus, it appears that nucleation and particle growth must be the rate-determining processes. Shorter nucleation (induction) times and/or faster particle growth rates will therefore lead to faster gelation from the sol state.[38] The loading and gap setting procedure in rheometric measurements takes around 2 min; therefore, the first set of data points, where gel network formation has been observed, is obtained at around 7.5 min after the dissolved gel (clear sol) has been removed from heat. This implies that nucleation and particle growth are very fast under these specific conditions, viz. cooling under ambient conditions, gentle shaking, transference from the sample vial to the rheometer, and preshear using large oscillatory strain at a frequency of 1 Hz for 30 s. Gelation times determined by inverting the sample vial (the gel time is estimated visually as the time at which the sample is unable to flow when the vial is inverted) are usually substantially longer than 10 min. This discrepancy is presumed to be a consequence of the large difference in sample volumes between the two experiments and the fact that the precise thermomechanical history has a profound effect on the gelation kinetics, particularly the nucleation rate. Indeed, this presumption is supported by visual observations and time-resolved dynamic light scattering experiments (vide infra). This strong dependence on thermomechanical history is also the origin of the poor reproducibility in kinetic experiments from run to run. To minimize such effects, it is paramount to follow precisely the same procedure for sample cooling and loading into the rheometer. In addition, gels formed via the mechanism described above, viz. nucleation, particle growth, flocculation, and coalescence, are intrinsically inhomogeneous systems, in which a supercooled, macroscopically homogeneous equilibrium sol phase is transformed into a metastable, microscopically inhomogeneous phase. The time course for such a transformation involves complex kinetics, since all four mechanistic processes discussed above may occur simultaneously during most of the gelation process. Therefore, after the initial formation of an immature gel network, the maturation process may involve further nucleation of particles as well as growth and flocculation of existing particles, all contributing to the overall evolution of interparticle bonding. It therefore seems inevitable that, even if the thermomechanical history is perfectly reproduced, the end result will be a gel network with intrinsically variable morphology and properties. By controlling the formation history, it is hoped that the resulting structure and properties can be specified within narrowly defined limits.

Time-Resolved Dynamic Light Scattering. Light scattering is a powerful technique to probe the structural changes occurring during the sol−gel transition and the kinetics of gelation. Analysis of the temporal fluctuations in scattered intensity (dynamic light scattering) probes the motion of the particle clusters and local network relaxation.[39] In time-resolved static and dynamic light scattering, several discrete phenomena,[40] such as an increase in the scattered intensity (occurrence of speckle patterns), a suppression of the initial amplitude of the intensity correlation function, and an increase in the relaxation time, typically signal the transformation of a sol into a gel. Here, time-resolved dynamic scattering was performed in an attempt to probe the sol gel transition point and the kinetics of the gelation as well as their dependence on thermomechanical history.

We found that the gelation times, measured from the onset of an increase in scatered intensity, are exceptionally sensitive to the sample history. Filtration, preshaking, and rotation of the sample cell during the gelation process all influence the gelation time. For example, studies examining the variation in scattered intensity (Supporting Information), $\langle I \rangle$, during gelation of a sample, after passage through a 450 nm membrane filter, were carried out. With preshaking applied for 5 min, a long induction period of about 12 h was observed, after which $\langle I \rangle$ increased abruptly. In contrast, when an identical sample was preshaken for 15 min, $\langle I \rangle$ was observed to increase without a detectable induction period. This is consistent with prior rheological and morphological evidence that the gelation kinetics, which depends on the crystal nucleation rate, is very sensitive to the thermomechanical history. Increased mechanical perturbation tends to result in faster nucleation rate and gel formation.[14] In the case of light scattering analysis, prior filtration of the sample may remove particulate impurities as well as nascent nuclei and consequently lead to a decrease in nucleation rate because of a decrease in the number of nucleation sites.

Thus, these light scattering experiments show that the nucleation rate, presumed inversely proportional to the induction period, is very dependent on the thermomechanical history of the samples and increases with increased mechanical agitation applied to the sample. Rheologically, the gel point appears to occur at some time after the initial increase in $\langle I \rangle$, but a precise correlation could not be made. However, after the initial increase in $\langle I \rangle$, a discrete change in dynamic light scattering properties is also observed, i.e., a suppression of the initial amplitude of the correlation function relative to the baseline, indicating the appearance of static inhomogeneities in the gel structure which increase in concentration with time. This event has been identified as the gel point by previous investigators.[39,40] The precise nature of these inhomogeneities is not clear, but it seems likely that they correspond to agglomerates of growing particles which reach a size where Brownian motion ceases.

Conclusions

Utilizing mixed solvent systems consisting of a good solvent (DMSO) with either a nonsolvent (water) or poor solvent (ethylene glycol), a systematic variation in the morphology of a class of stimuli-responsive gels, formed by a metallosupramolecular polymer, **1:Zn**, was achieved. In each solvent system, a composition window is located in which gels are formed, varying in turbidity from highly opaque (water- or ethylene glycol-rich) to highly transparent (DMSO-rich). Outside this window, either precipitation (poor solvent-rich) or solubilization (good solvent-rich) occurs. Morphological and dynamic light scattering evidence suggests gelation occurs by a common mechanism throughout the composition range, i.e., via the

flocculation of semicrystalline colloidal particles. Increase of DMSO content leads to a reduction in the particle size, refractive index contrast, and degree of crystallinity, accompanied by an evolution to a lamellar organization as well as an increase in sol concentration and in gel transparency. These changes in structure and morphology are accompanied by an increase in the shear storage modulus of the gel up to a maximum value, beyond which the modulus decreases. Thus, by tailoring the solvent composition, it is possible to produce highly transparent gels, which are very strong but which are also highly mechano-responsive; i.e., they exhibit pronounced yielding and thixotropic behavior. Both uniform (spherical) and irregular colloidal particles can be observed in opaque gel samples. On the basis of time-resolved optical microscopy of the evolution of particle morphology during gelation, it seems likely that the uniform particles result primarily from nucleation and growth of a single particle, although a particle fusion mechanism cannot be completely discounted, whereas the irregular particles are formed via secondary nucleation on primary particles and/or impingement of growing primary particles. Rheological analysis shows that on application of sufficient mechanical stress these gels exhibit brittle failure to form a transparent free-flowing liquid, and that the gel state reforms essentially instantaneously upon removal of the stress. Gelation kinetics was found to be very dependent on thermomechanical history of the samples; i.e., mechanical perturbation and thermal quenching each lead to much faster gel formation.

Acknowledgment. This material is based upon work supported by the National Science Foundation, under Grant CAREER-CHE0133164, CHE-0704026, and DMR 0513010, Polymers Program. The authors are grateful to Prof. Patrick Mather for use of the Anton Paar MCR 501 rheometer, Olivier Arnoult and Timothy Marsh for assistance with rheometric experiments, Dr. J. Benjamin Beck for discussions, and Dr. David Hovis for laser scanning confocal microscopy assistance.

Supporting Information Available: Experimental details of sample preparation and additional experimental results (photography of concentration-dependent gelation, DIC and POM images of variation in gel morphology with solvent composition, time-resolved DIC images of morphology evolution during gelation, XRD and DSC of gels as a function of solvent composition, and time-resolved light scattering intensity during gelation). This material is available free of charge via the Internet at http://pubs.acs.org.

References and Notes

(1) (a) Brunsveld, L.; Folmer, B. J. B.; Meijer, E. W.; Sijbesma, R. P. *Chem. Rev.* **2001**, *101*, 4071–4097. (b) Ciferri, A. *Macromol. Rapid Commun.* **2002**, *23*, 511–529. (c) *Supramolecular Polymers*, 2nd ed.; Ciferri, A., Ed.; CRC: Boca Raton, FL, 2005. (d) Brunsveld, L.; Folmer, B. J. B.; Meijer, E. W. *MRS Bull.* **2000**, *25*, 49–53. (e) Fogleman, E. A.; Yount, W. C.; Xu, J.; Craig, S. L. *Angew. Chem., Int. Ed.* **2002**, *41*, 4026–4028. (f) Serpe, M. J.; Craig, S. L. *Langmuir* **2007**, *23*, 1626–1634.

(2) (a) Yount, W. C.; Loveless, D. M.; Craig, S. L. *J. Am. Chem. Soc.* **2005**, *127*, 14488–14496. (b) Loveless, D. M.; Jeon, S. L.; Craig, S. L. *Macromolecules* **2005**, *38*, 10171–10177. (c) Bodenthin, Y.; Pietsch, U.; Grenzer, J.; Geue, T.; Mo1hwald, H.; Kurth, D. G. *J. Phys. Chem. B* **2005**, *109*, 12795–12799. (d) Yount, W. C.; Loveless, D. M.; Craig, S. L. *Angew. Chem., Int. Ed.* **2005**, *44*, 2746–2748.

(3) (a) Lestage, D. J.; Yu, M.; Urban, M. W. *Biomacromolecules* **2005**, *6*, 1561–1572. (b) Ionov, L.; Minko, S.; Stamm, M.; Gohy, J. F.; Jerome, R.; Scholl, A. *J. Am. Chem. Soc.* **2003**, *125*, 8302–8306. (c) Stayton, P. S.; Shimoboji, T.; Long, C.; Chilkoti, A.; Chen, G. H.; Harris, J. M.; Hoffman, A. S. *Nature (London)* **1995**, *378*, 472–474. (d) Delaire, J. A.; Nakatani, K. *Chem. Rev.* **2000**, *100*, 1817–1846. (e) Hugel, T.; Holland, N. B.; Cattani, A.; Moroder, L.; Seitz, M.; Gaub, H. E. *Science* **2002**, *296*, 1103–1106. (f) Li, Y.; He, Y.; Tong, X.; Wang, X. *J. Am. Chem. Soc.* **2005**, *127*, 2402–2403. (g) Barker, S. L. R.; Ross, D.; Tarlov, M. J.; Gaitan, M.; Locascio, L. E. *Anal. Chem.* **2000**, *72*, 5925–5929. (h) Kikuchi, A.; Okano, T. *Adv. Drug Delivery Rev.* **2002**, *54*, 53–77. (i) Cunliffe, D.; de las Heras Alarcon, C.; Peters, V.; Smith, J. R.; Alexander, C. *Langmuir* **2003**, *19*, 2888–2899. (j) Hoffmann, J.; Plotner, M.; Kuckling, D.; Fischer, W. J. *Sens. Actuators, A* **1999**, *77*, 139–144. (k) Urry, D. W. *Biopolymers* **1998**, *47*, 167–178.

(4) (a) Kastner, U. *Colloids Surf., A* **2001**, *183*−*185*, 805–821. (b) Yao, N.; Jamieson, A. M. *Polymer* **2000**, *41*, 1992–2000.

(5) Lehn, J.-M. *Supramolecular Chemistry*; VCH: Weinheim, 1995.

(6) (a) Zimmerman, S. C.; Zeng, F. W.; Reichert, D. E. C.; Kolotuchin, S. V. *Science* **1996**, *271*, 1095–1098. (b) Castellano, R. K.; Nuckolls, C.; Eichhorn, S. H.; Wood, M. R.; Lovinger, A. J.; Rebek, J., Jr. *Angew. Chem., Int. Ed.* **1999**, *38*, 2603–2606. (c) Sijbesma, R. P.; Beijer, F. H.; Brunsveld, L.; Folmer, B. J. B.; Hirschberg, J. H. K. K.; Lange, R. F. M.; Lowe, J. K. L.; Meijer, E. W. *Science* **1997**, *278*, 1601–1604. (d) Xu, J.; Fogleman, E. A.; Craig, S. L. *Macromolecules* **2004**, *37*, 1863–1870. (e) Keizer, H. M.; Sijbesma, R. P.; Jansen, J. F. G. A.; Pasternack, G.; Meijer, E. W. *Macromolecules* **2003**, *36*, 5602–5606.

(7) (a) Hinderberger, D.; Schmelz, O.; Rehahn, M.; Jeschke, G. *Angew. Chem., Int. Ed.* **2004**, *43*, 4616–4621. (b) Schmatloch, S.; van den Berg, A. M. J.; Alexeev, A. S.; Hofmeier, H.; Schubert, U. S. *Macromolecules* **2003**, *36*, 9943–9949. (c) Dobrawa, R.; Lysetska, M.; Ballester, P.; Grune, M.; Wurthner, F. *Macromolecules* **2005**, *38*, 1315–1325. (d) Kurth, D. G.; Meister, A.; Thuenemann, A. F.; Foerster, G. *Langmuir* **2003**, *19*, 4055–4057. (e) Vermonden, T.; van Steenbergen, M. J.; Besseling, N. A. M.; Marcelis, A. T. M.; Hennink, W. E.; Sudhoelter, E. J. R.; Cohen Stuart, M. A. *J. Am. Chem. Soc.* **2004**, *126*, 15802–15809. (f) Yount, W. C.; Juwarker, H.; Craig, S. L. *J. Am. Chem. Soc.* **2003**, *125*, 15302–15303. (g) Paulusse, J. M. J.; Sijbesma, R. P. *Angew. Chem., Int. Ed.* **2004**, *43*, 4460–4462. (h) Colombani, O.; Baroiz, C.; Bouteiller, L.; Chane'ac, C.; Fromperie, L.; Lortie, F.; Montes, H. *Macromolecules* **2005**, *38*, 1752–1759. (i) Nishihara, H.; Shimura, T.; Ohkubo, A.; Matsuda, N.; Aramaki, K. *Adv. Mater.* **1993**, *5*, 752–754. (j) Constable, E. C. *Chem. Commun.* **1997**, 1073–1080. (k) Lohmeijer, B. G. G.; Schubert, U. S. *J. Polym. Sci., Part A: Polym. Chem.* **2003**, *41*, 1413–1427. (l) Schmatloch, S.; van den Berg, A. M. J.; Hofmeier, H.; Schubert, U. S. *Des. Monomers Polym.* **2004**, *7*, 191–201. (m) Hofmeier, H.; Schmatloch, S.; Wouters, D.; Schubert, U. S. *Macromol. Chem. Phys.* **2003**, *204*, 2197–2203. (n) Schubert, U. S.; Eisenbach, C. D. *Angew. Chem., Int. Ed.* **2002**, *41*, 2892–2926. (o) Kim, H. J.; Lee, J. H.; Lee, M. *Angew. Chem., Int. Ed.* **2005**, *44*, 5810–5814. (p) Gerhardt, W. W.; Zucchero, A. J.; South, C. R.; Bunz, U. H. F.; Weck, M. *Chem.*−*Eur. J.* **2007**, *13*, 4467–4474. (q) South, C. R.; Higley, M. N.; Leung, K. C.-F.; Lanari, D.; Nelson, A.; Grubbs, R. H.; Stoddart, J. F.; Weck, M. *Chem.*−*Eur. J.* **2006**, *12*, 3789–3797. (r) South, C. R.; Burd, C.; Weck, M. *Acc. Chem. Res.* **2007**, *40*, 63–74.

(8) (a) Beck, J. B.; Ineman, J. M.; Rowan, S. J. *Macromolecules* **2005**, *38*, 5060–5068. (b) Iyer, P. K.; Beck, J. B.; Weder, C.; Rowan, S. J. *Chem. Commun.* **2005**, 319–321. (c) Knapton, D.; Rowan, S. J.; Weder, C. *Macromolecules* **2006**, *39*, 651–657.

(9) Dobrawa, R.; Würthner, F. *J. Polym. Sci., Part A: Polym. Chem.* **2005**, *43*, 4981–4995.

(10) (a) Beck, J. B.; Rowan, S. J. *J. Am. Chem. Soc.* **2003**, *125*, 13922–13923. (b) Rowan, S. J.; Beck, J. B. *Faraday Discuss.* **2005**, *128*, 43–53. (c) Zhao, Y.; Beck, J. B.; Rowan, S. J.; Jamieson, A. M. *Macromolecules* **2004**, *37*, 3529–3530. (d) Weng, W.; Beck, J. B.; Jamieson, A. M.; Rowan, S. J. *J. Am. Chem. Soc.* **2006**, *128*, 11663–11672. (e) Weng, W.; Beck, J. B.; Jamieson, A. M.; Rowan, S. J. *Tetrahedron* **2007**, *63*, 7419–7431.

(11) (a) Kelch, S.; Rehahn, M. *Macromolecules* **1997**, *30*, 6185–6193. (b) Chen, H. C.; Cronin, J. A.; Archer, R. D. *Macromolecules* **1994**, *27*, 2174–2180. (c) Lahn, B.; Rehahn, M. *e-Polym.* **2002**, *1*, 1–33.

(12) (a) Oh, M.; Mirkin, C. A. *Nature (London)* **2005**, *438*, 651–654. (b) Oh, M.; Mirkin, C. A. *Angew. Chem., Int. Ed.* **2006**, *45*, 5492–5494. (c) Jeon, Y. M.; Heo, J.; Mirkin, C. A. *J. Am. Chem. Soc.* **2007**, *129*, 7480–7481.

(13) (a) Sun, X.; Dong, S.; Wang, E. *J. Am. Chem. Soc.* **2005**, *127*, 13102–13103. (b) Wei, H.; Li, B. L.; Du, Y.; Dong, S. J.; Wang, E. *Chem. Mater.* **2007**, *19*, 2987–2993. (c) Maeda, H.; Hasegawa, M.; Hashimoto, T.; Kakimoto, T.; Nishio, S.; Nakanishi, T. *J. Am. Chem. Soc.* **2006**, *128*, 10024–10025. (d) Park, K. H.; Jang, K.; Son, S. U.; Sweigart, D. A. *J. Am. Chem. Soc.* **2006**, *128*, 8740–8741.

(14) Mullin, J. W. *Crystallization*, 3rd ed.; Butterworth-Heinemann: Oxford, 1993.

(15) (a) Hirst, A. R.; Smith, D. K.; Harrington, J. P. *Chem.*−*Eur. J.* **2005**, *11*, 6552–6559. (b) Hirst, A. R.; Smith, D. K. *Chem.*−*Eur. J.* **2005**, *11*, 5496–5508. (c) Schneider, J. P.; Pochan, D. J.; Ozbas, B.; Rajagopal, K.; Pakstis, L.; Kretsinger, J. *J. Am. Chem. Soc.* **2002**, *124*, 15030–15037.

(16) Song, A.; Dong, S.; Jia, X.; Hao, J.; Liu, W.; Liu, T. *Angew. Chem.* **2005**, *117*, 4086–4089.

(17) Russel, W. B.; Saville, D. A.; Schowalter, W. R. *Colloidal Dispersions*; Cambridge University: Cambridge, 1989.
(18) Macosko, C. W. *Rheology: Principles, Measurements and Applications*; VCH: New York, 1994.
(19) Barnes, H. A.; Hutton, J. F.; Walters, K. *An Introduction to Rheology*; Elsevier: Amsterdam, **1989**.
(20) Bradbury, A.; Goodwin, J. W.; Hughes, R. W. *Langmuir* **1992**, *8*, 2863–2872.
(21) (a) Yziquel, F.; Carreau, P. J.; Tanguy, P. A. *Rheol. Acta* **1999**, *38*, 14–25. (b) Yziquel, F.; Carreau, P. J.; Moan, M.; Tanguy, P. A. *J. Non-Newtonian Fluid Mech.* **1999**, *86*, 133–155.
(22) (a) Walls, H. J.; Caines, B.; Sanchez, A. M.; Khan, S. A. *J. Rheol.* **2003**, *47*, 847–868. (b) Nakamura, H.; Tachi, K. *J. Appl. Polym. Sci.* **2001**, *79*, 1627–1638. (c) Craciun, L.; Carreau, P. J.; Heuzey, M.; van de Ven, T.; Moan, M. *Rheol. Acta* **2003**, *42*, 410–420. (d) Yang, M.-C.; Scriven, L. E.; Macosko, C. W. *J. Rheol.* **1986**, *30*, 1015–1029. (e) Roland, C. M. *J. Rheol.* **1990**, *34*, 25–34.
(23) (a) Shih, W.; Shih, W. Y.; Kim, S.; Liu, J.; Aksay, I. A. *Phys. Rev. A* **1990**, *42*, 4772–4780. (b) Shih, W.; Shih, W. Y.; Aksay, I. A. *J. Am. Ceram. Soc.* **1999**, *82*, 616–624.
(24) Mewis, J. *J. Non-Newtonian Fluid Mech.* **1979**, *6*, 1–20.
(25) Nguyen, Q. D.; Boger, D. V. *Rheol. Acta* **1985**, *24*, 427–437.
(26) Nguyen, Q. D.; Boger, D. V. *J. Rheol.* **1983**, *27*, 321–349.
(27) Burns, J. L.; Yan, Y.; Jameson, G. J.; Biggs, S. *Colloids Surf.* **2003**, *214*, 173–180.
(28) Cracium, L.; Carreau, P. J.; Heuzey, M.; van de Ven, T.; Moan, M. *Rheol. Acta* **2003**, *42*, 410–420.
(29) Daniel, C.; Dammer, C.; Guenet, J.-M. *Polymer* **1994**, *35*, 4243–4246.
(30) Goodwin, J. W. *Rheology for Chemists: An Introduction*; Royal Society of Chemistry: Cambridge, 2000.
(31) Buscall, R.; McGowan, J. I.; Morton-Jones, A. J. *J. Rheol.* **1993**, *37*, 621–641.
(32) Russel, W. B.; Grant, M. C. *Colloids Surf., A* **2000**, *161*, 271–282.
(33) Walls, H. J.; Caines, S. B.; Sanchez, A. M.; Khan, S. A. *J. Rheol.* **2003**, *47*, 847–868.
(34) Becu, L.; Grondin, P.; Colin, A.; Manneville, S. *Colloids Surf., A* **2004**, *263*, 146–152.
(35) Tari, G. *Am. Ceram. Soc. Bull.* **2003**, *82*, 43–47.
(36) Yu, B. C.; Lange, F. F. *Adv. Mater.* **2001**, *13*, 276–280.
(37) Xie, B. J.; Parkhill, R. L.; Warren, W. L.; Smay, J. E. *Adv. Funct. Mater.* **2006**, *16*, 1685–1693.
(38) (a) Terech, P.; Weiss, R. G. *Chem. Rev.* **1997**, *97*, 3133–3159. (b) Huang, X.; Terech, P.; Raghavan, S. R.; Weiss, R. G. *J. Am. Chem. Soc.* **2005**, *127*, 4336–4344. (c) Huang, X.; Raghavan, S. R.; Terech, P.; Weiss, R. G. *J. Am. Chem. Soc.* **2006**, *128*, 15341–15352.
(39) (a) Bergenholtz, J.; Fuchs, M. *Phys. Rev. E* **1999**, *59*, 5706–5715. (b) Xue, J. Z.; Pine, D. J.; Milner, S. T.; Wu, X. L.; Chaikin, P. M. *Phys. Rev. A* **1992**, *46*, 6550–6563. (c) Shibayama, M.; Norisuye, T. *Bull. Chem. Soc. Jpn.* **2002**, *75*, 641–659.
(40) (a) Boyko, V.; Richter, S. *Macromol. Chem. Phys.* **2004**, *205*, 724–730. (b) Dastidar, P.; Okabe, S.; Nakano, K.; Iida, K.; Miyata, M.; Tohnai, N.; Shibayama, M. *Chem. Mater.* **2005**, *17*, 741–748. (c) Norisuye, T.; Inoue, M.; Shibayama, M.; Tamaki, R.; Chujo, Y. *Macromolecules* **2000**, *33*, 900–905. (d) Shibayama, M.; Fujikawa, Y.; Nomura, S. *Macromolecules* **1996**, *29*, 6535–6540.

MA801046W